American Mineralogist, Volume 81, pages 369–374, 1996

Monoclinic-orthorhombic phase transition in the $K_2MgSi_5O_{12}$ leucite analog

SIMON A.T. REDFERN[1] AND C. MICHAEL B. HENDERSON[2]

[1]Department of Earth Sciences, University of Cambridge, Downing Street, Cambridge CB2 3EQ, U.K.
[2]Department of Earth Sciences, University of Manchester, Oxford Road, Manchester M13 9PL, U.K.

ABSTRACT

The high-temperature cell parameters of $K_2MgSi_5O_{12}$ have been measured by X-ray powder diffraction between room temperature and 842 K. A first-order ferroelastic phase transition between the room-temperature $P2_1/c$ structure and a high-temperature *Pbca* structure occurs at 622 K. The spontaneous strain behaves as the order parameter for the transition, following a simple Landau model. Simple lattice dynamics simulation of the magnesiosilicate framework reveals that acoustic mode softening drives the elastic instability. The first-order character of the transition is attributed to a large excess volume, which arises from collapse of the framework around the alkali site. At higher temperatures the orthorhombic cell edges converge toward a metrically cubic structure, but this transformation requires Mg-Si disorder, which was not observed on the time scale of these experiments.

FERROELASTICITY AND ORDER-DISORDER IN LEUCITE-RELATED FRAMEWORKS

The leucite framework structure represents an extremely stable topological arrangement. Recent studies have shown that, although comparatively insignificant in nature, the known chemical extent of the leucite family of $X^{I}(Y^{II}_{x}Z^{III}_{1-2x})Si_{2+x}O_6$ ($0 < x < 0.5$) compounds is expanding rapidly, with over 50 such compounds reported (Torres-Martinez and West 1989; Kohn et al. 1994). Recent investigations of leucite-related compounds have, for example, focused on their catalytic properties, especially those with transition metals substituting for Al and Si in the aluminosilicate tetrahedral framework (Heinrich and Baerlocher 1991). Investigations of synthetic leucite analogs with X = K, Rb, Cs; Y = Mg, Zn, Cu, Cd; Z = Al, Fe have revealed a range of symmetrically distinct structures with the same leucite topology (Bell et al. 1994a, 1994b; Bell and Henderson 1994). These studies have highlighted the possible occurrence of three structural phenomena within anhydrous leucite and its related compounds: (1) Instabilities of the tetrahedral framework may lead to displacive transitions, (2) ordering of tetrahedral cations may occur on the T sites, and (3) the size and dynamic behavior of the alkali cation in the "W" site may influence either of the above processes (for details of leucite-site nomenclature and a more general discussion of the leucite structure type the reader is referred to the review by Galli et al. 1978).

Of these, the role of Al-Si order-disorder in natural leucite, and its relation to displacive distortions, has been the subject of much recent attention. In contrast to other framework aluminosilicates, in which strong coupling is often observed between displacive instabilities and Al-Si ordering [e.g., in feldspars, see Salje (1990) or Redfern (1995) for a review], it now seems clear that long-range Al-Si order is only weakly coupled (if at all) to the displacive cubic-tetragonal phase transition in $KAlSi_2O_6$ leucite (Dove et al. 1993). Dove et al. (1996) attributed this to a low ordering temperature for leucite, which they associated with dilution of Al in the tetrahedral network (in comparison with an Al:Si ratio of 1:1). On the basis of calculations of the exchange interaction for ordering, J_1 (equal to the energy difference between an Al-O-Al linkage plus Si-O-Si as against two Al-O-Si linkages), and estimates of the second-nearest-neighbor interaction, J_2, they used a modified Bragg-Williams approach to arrive at an order-disorder transition for leucite of 300 °C. They argued that the sluggishness of Al-Si ordering kinetics below such a low T_c renders the process insignificant in leucite and explains why long-range Al-Si ordering is so limited in this mineral.

Tetrahedral cation ordering is observed in certain leucite analogs, however. For example, although it appears that Al^{3+} shows only limited ordering over the three T sites of natural $I4_1/a$ $KAlSi_2O_6$, studies of synthetic Fe analogs ($KFeSi_2O_6$) show that Fe^{3+} tends to order preferentially on T_3 and T_2 rather than T_1 (Bell and Henderson 1994; Brown et al. 1987). More dramatic, however, is the behavior of tetrahedral cations in certain $K_2Y^{2+}Si_5O_{12}$ leucite analogs (Y^{2+} = Mg, Zn, and Cd; Bell et al. 1993; Kohn et al. 1994). When synthesized hydrothermally at relatively low temperatures each of these compounds crystallizes as a well-ordered low-symmetry leucite framework, whereas high-temperature dry synthesis from oxides tends to yield disordered structures, isomorphous with the *Ia3d* high-temperature structure of natural $KAlSi_2O_6$. Coupling between tetrahedral ordering and macroscopic strain in these leucite analogs is very strong indeed, as is evidenced by crystallization of or-

0003–004X/96/0304–0369$05.00

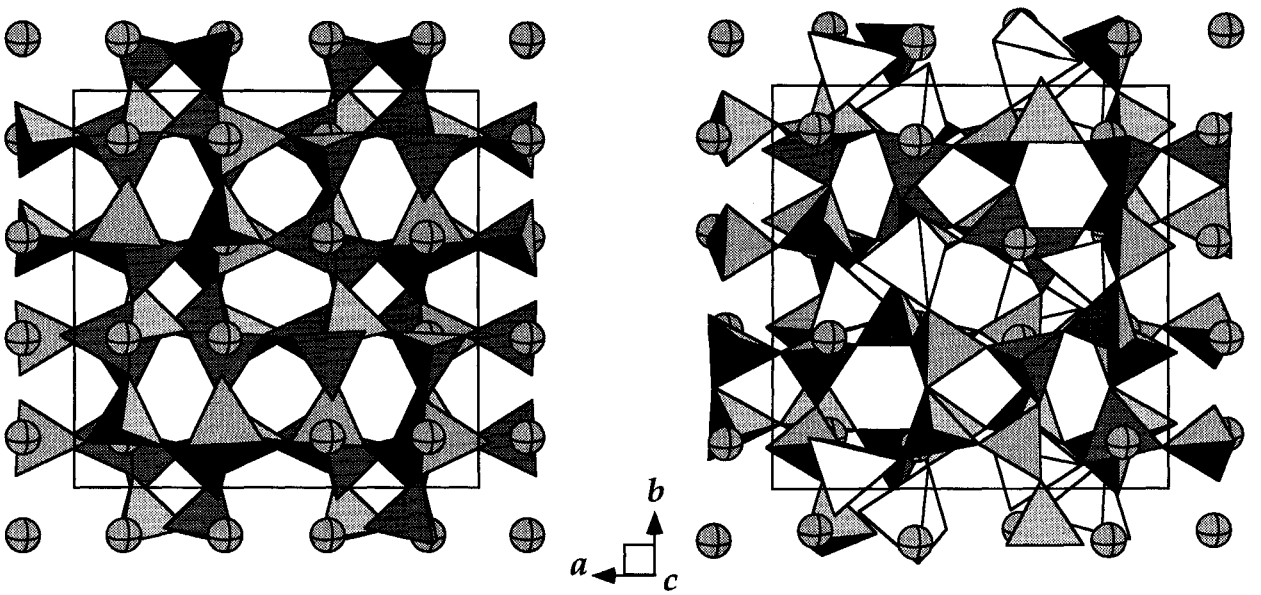

FIGURE 1. Crystal structures of the monoclinic (right) and cubic (left) polymorphs of the $K_2MgSi_5O_{12}$ leucite analog. K atoms are shown as circles, MgO_4 tetrahedra are shown unshaded, and SiO_4 tetrahedra (and TO_4 tetrahedra in the disordered cubic phase) are shown shaded.

dered polymorphs in low-symmetry monoclinic and orthorhombic structures with strains of a few percent compared with the disordered *Ia3d* aristotype. Why does their behavior appear to be so different from that of natural $KAlSi_2O_6$ leucite?

The arguments of Dove et al. (1996) point to dilution of Al with respect to the ideal 1:1 Al:Si ratio (pertinent to traditional Bragg-Williams models) as the reason for the low ordering temperature of $KAlSi_2O_6$. It seems paradoxical, therefore, that the $K_2Y^{2+}Si_5O_{12}$ ordered leucite analogs have Y:Si ratios corresponding to even greater dilution, yet they seem to have higher temperature order-disorder transitions. To provide further light on the nature and role of order-disorder, its dependence on T-site chemistry, and its coupling to elastic transitions in these framework structures, we studied the high-temperature behavior of the $K_2MgSi_5O_{12}$ leucite analog. This material is related to natural leucite by the coupled substitution

$$2Al^{3+} \leftrightarrow Mg^{2+} + Si^{4+}. \quad (1)$$

The relationship between the tetrahedrally ordered $P2_1/c$ structure and the disordered *Ia3d* polymorph of this compound is illustrated in Figure 1. The hydrothermally synthesized monoclinic polymorph has 12 symmetrically distinct tetrahedral sites, whereas the cubic structure has just one. Another leucite-related compound ($Cs_2CdSi_5O_{12}$) crystallizes as an ordered *Pbca* structure, with six T sites, and possible relations among these polymorphs are shown in Figure 2. It is clear that order-disorder processes and ferroelastic phase transitions both play important roles in controlling the high-temperature behavior of these materials.

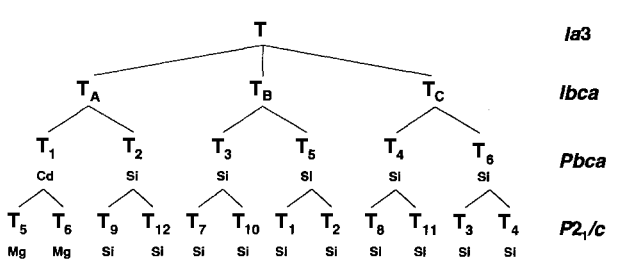

FIGURE 2. Relationships among tetrahedral sites in the monoclinic $K_2MgSi_5O_{12}$ leucite analog and its higher symmetry parents. Site occupancies for $P2_1/c$ $K_2MgSi_5O_{12}$ and *Pbca* $Cs_2CdSi_5O_{12}$ are from Bell et al. (1994a, 1994b). The transitions between $P2_1/c$-*Pbca* and *Ibca*-*Ia*3 are expected to be displacive in character, whereas *Pbca*-*Ibca* involves order-disorder of the tetrahedral cations.

HIGH-TEMPERATURE POWDER DIFFRACTION OF $K_2MgSi_5O_{12}$

The sample used for the high-temperature study was from the same batch studied by Bell et al. (1994b) and Kohn et al. (1994) and was crystallized from glass by hydrothermal synthesis at 600 °C and 0.5 kbar for 7 d. High-temperature powder X-ray diffraction patterns were collected between room temperature and 842 K using a Huber high-temperature Guinier camera. Monochromatic Cu$K\alpha_1$ radiation was selected from a bent quartz monochromator. Diffraction patterns were collected on single-sided emulsion film from a thin powdered sample held in a platinum wire loop in transmission geometry.

TABLE 1. High-temperature cell parameters of $K_2MgSi_5O_{12}$

T (K)	a (Å)	b (Å)	c (Å)	β (°)	V (Å³)
293	13.166(5)	13.648(7)	13.062(6)	91.74(3)	2346.0(1.2)
319	13.166(7)	13.655(6)	13.068(7)	91.72(4)	2348.2(1.4)
346	13.174(6)	13.658(8)	13.073(8)	91.69(4)	2351.2(1.5)
372	13.176(7)	13.656(6)	13.084(7)	91.68(4)	2353.2(1.4)
399	13.182(7)	13.654(8)	13.095(8)	91.66(4)	2355.9(1.5)
424	13.204(7)	13.659(9)	13.101(8)	91.60(4)	2361.8(1.6)
449	13.209(7)	13.655(8)	13.121(8)	91.52(4)	2365.6(1.5)
475	13.231(7)	13.656(7)	13.130(7)	91.50(4)	2371.6(1.4)
500	13.233(5)	13.654(6)	13.141(6)	91.50(3)	2373.4(1.1)
525	13.251(5)	13.646(5)	13.151(6)	91.43(3)	2377.2(1.2)
549	13.267(6)	13.644(8)	13.172(8)	91.37(4)	2383.6(1.5)
574	13.276(5)	13.633(7)	13.190(6)	91.31(3)	2386.6(1.3)
598	13.296(5)	13.641(6)	13.199(5)	91.28(3)	2393.3(1.1)
623	13.315(6)	13.637(8)	13.215(7)	91.26(3)	2399.0(1.3)
647	13.340(6)	13.613(7)	13.237(7)	91.19(3)	2403.1(1.2)
650	13.328(5)	13.610(7)	13.234(6)	91.16(3)	2400.2(1.3)
654	13.339(6)	13.617(7)	13.244(7)	91.14(3)	2405.0(1.3)
657	13.345(5)	13.627(7)	13.255(6)	91.14(3)	2409.8(1.2)
661	13.369(6)	13.634(6)	13.265(5)	91.13(3)	2417.4(1.2)
664	13.430(6)	13.697(6)	13.357(6)	90.0	2457.1(1.3)
668	13.418(3)	13.689(3)	13.371(4)	90.0	2456.0(0.7)
670	13.419(6)	13.684(5)	13.368(5)	90.0	2454.7(1.3)
709	13.434(9)	13.675(9)	13.377(8)	90.0	2457.6(1.8)
740	13.441(7)	13.672(7)	13.390(6)	90.0	2460.5(1.4)
775	13.453(6)	13.670(7)	13.400(6)	90.0	2464.1(1.3)
809	13.464(7)	13.666(7)	13.421(6)	90.0	2469.3(1.4)
842	13.485(7)	13.662(7)	13.422(6)	90.0	2472.7(1.5)

Note: Figures in parentheses represent one standard-deviation error.

Si powder was mixed with the sample to act as an internal 2θ standard, enabling film shrinkage corrections and zero-point corrections to be made for each exposure. The furnace stability was better than ± 1 K at the lower range of the heating experiments, worsening to ± 2 K at the upper end of the temperature range, with the control thermocouple positioned < 1 mm from the sample. The set temperatures were independently calibrated by a secondary type-K thermocouple placed in the sample position. Diffraction patterns were collected under isothermal conditions at varying temperature intervals (Table 1), but an additional continuous heating film was recorded, which shows the behavior of Bragg reflections on heating through the temperature interval of interest in this material (Fig. 3).

Films were scanned on a flat-bed scanner and positions of Bragg reflections were determined in a manner like that described by O'Neill et al. (1993). The temperature evolution of the 400, 040, and 004 group of peaks reveals the first-order nature of the phase transition, showing coexisting monoclinic and orthorhombic peaks at $T_c \pm 20$ K (Fig. 4) and a step in peak positions. Typically, approximately 30 Bragg peaks below 60° 2θ were measured and used for cell-parameter determination. Cell parameters were determined by least-squares refinement of measured 2θ positions, with maximum deviations between observed and calculated values $\leq 0.02°$ 2θ. The refined cell parameters are given in Table 1 and presented as a function of temperature in Figure 5. Discontinuities in all cell edges as well as the cell angle β are apparent at the transition point.

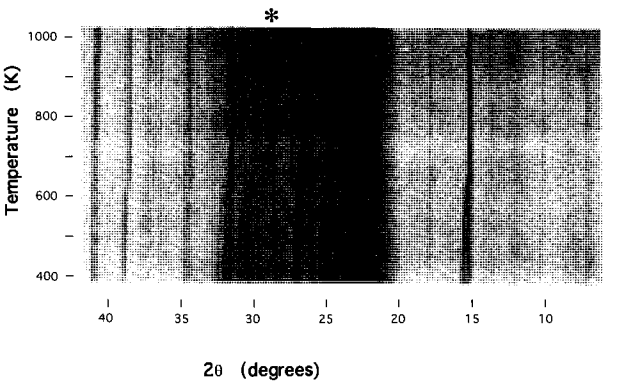

FIGURE 3. Continuous-heating diffraction patterns of ordered $K_2MgSi_5O_{12}$. Split pairs of peaks in the room-temperature monoclinic structure converge in the high-temperature orthorhombic structure. Orthorhombic peaks likewise converge to a higher symmetry structure on increasing temperature, but the material melts incongruently before a further transition occurs. The asterisk marks the position of an Si line.

ELASTIC INSTABILITY IN $K_2MgSi_5O_{12}$

The high-temperature powder diffraction patterns of $K_2MgSi_5O_{12}$ reveal a reversible nonquenchable phase transition from the room-temperature $P2_1/c$ space group to an orthorhombic structure at ~350 °C. The high-temperature phase is presumed to be *Pbca* from the symmetry relations described in Figure 2 and by analogy to the $Cs_2CdSi_5O_{12}$ isomorph. The transition is, therefore, potentially ferroelastic.

We performed a lattice dynamics simulation of the idealized tetrahedral framework of the *Pbca* structure using the CRUSH code described by Hammonds et al. (1994). This method reveals elastic instabilities inherent in the

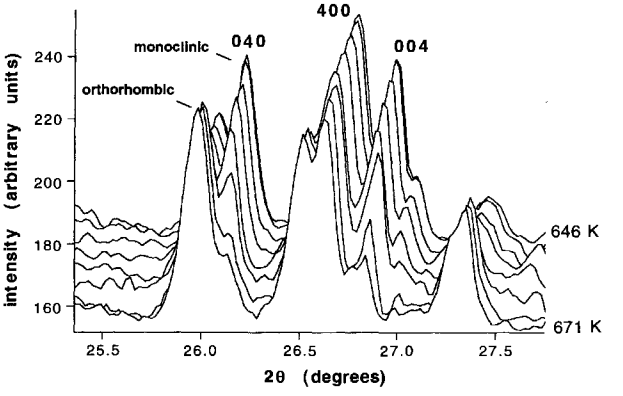

FIGURE 4. Scans of the 400, 040, and 004 group of peaks in monoclinic and orthorhombic $K_2MgSi_5O_{12}$ across the phase transition, obtained at equally spaced temperature intervals between 671 and 646 K. The coexistence of the two polymorphs across an extended temperature range near T_c and the step in peak position are both indicative of the first-order character of the transition.

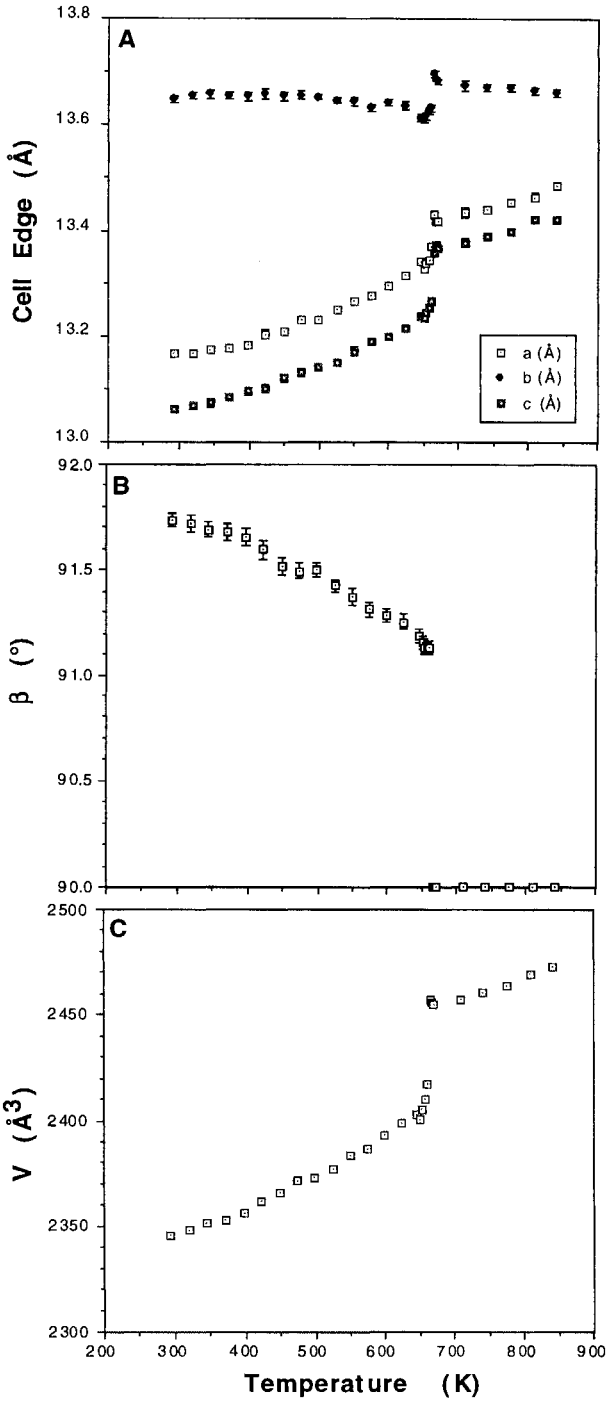

FIGURE 5. Temperature dependence of the cell edges, β angle, and volume (**A**, **B**, and **C**, respectively) of ordered $K_2MgSi_5O_{12}$. Error bars represent $\pm 1\sigma$.

magnesiosilicate framework resulting from its topological connectivity and provides an energy spectrum of the polyhedral tilt distortions, or rigid-unit modes, that the framework may undergo. Such rigid-unit mode analysis of our orthorhombic leucite structure reveals that the lowest lying acoustic branch of the tetrahedral framework, propagating along the [ζ0ζ] directions of k space, is anomalously soft (Fig. 6). This suggests that the transition can be explained in terms of simple acoustic mode softening, in which case the spontaneous strain arising below the phase transition, and revealed in the temperature-dependent lattice parameters, is the order parameter for the phase transition.

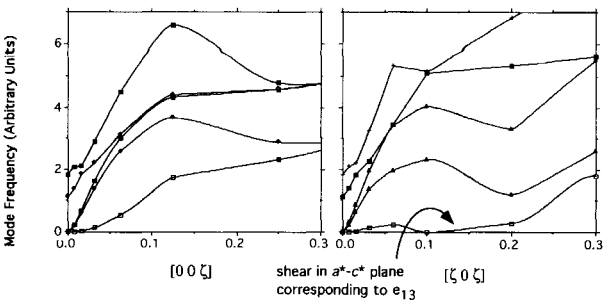

FIGURE 6. Lowest lying phonon-dispersion curves of an idealized tetrahedral framework of *Pbca* leucite from lattice dynamics calculations of the rigid-unit mode spectrum. The lowest lying branch in the [ζ0ζ] direction of the Brillouin zone displays significant softening along its length, demonstrating that the framework is susceptible to an acoustic instability.

The primary order parameter behaves as the symmetry-adapted strain, e_{13} (Aizu 1970). This shear strain was determined from the behavior of the monoclinic β angle, and its temperature dependence indicates that the transition is first order in character (Fig. 7). We employ a Landau model to describe the excess thermodynamic quantities at the phase transition (see Salje 1990). Assuming the simplest Landau potential of the form

$$\Delta G(Q) = \frac{A}{2}(T - T_C)Q^2 + \frac{B}{4}Q^4 + \frac{C}{6}Q^6 \qquad (2)$$

one obtains the fit shown by the solid line in Figure 7 for values of A/C = 1.17×10^{-9} K^{-1}, B/C = -5.17×10^{-4}, and T_c = 622 K.

The symmetry relations of the paraelastic and ferroelastic phases satisfy the Landau and Lifshitz criteria for a second-order phase transition, yet the observed behavior is clearly first order. If the transition corresponds to a simple acoustic shear, why is B so negative and thus the transition so strongly first order? The answer may lie in the behavior of the volume through the phase transition (Fig. 5C). A large negative excess volume arises below T_c, which renormalizes the Q^4 term in the Landau expansion, modifying B to negative values.

A similarly large volume strain occurs below the high-temperature tetragonal-cubic transition in $KAlSi_2O_6$ leucite, where it is associated with crumpling of the aluminosilicate framework and reduction in the volume of the irregular K^+ coordination polyhedron. By analogy with the behavior in $KAlSi_2O_6$, we presume that the large volume anomaly below the transition in $K_2MgSi_5O_{12}$ results from collapse of the framework around the alkali site in the monoclinic phase. This provides a mechanism for first-order behavior to dominate the high-temperature evolution of the phase transition; thus it is the alkali cat-

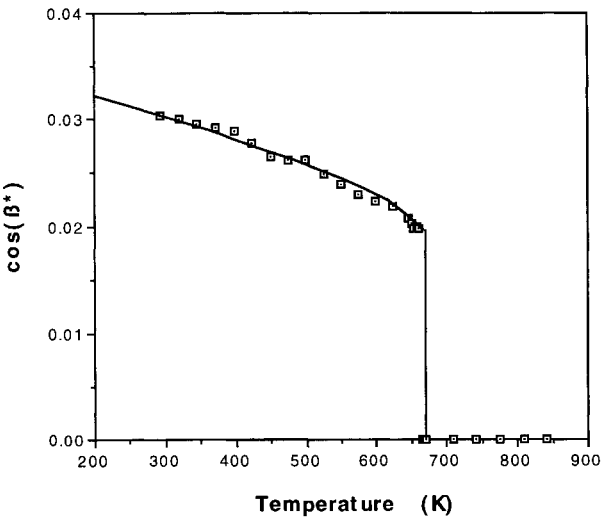

FIGURE 7. Temperature dependence of the spontaneous strain $e_{13} = \cos \beta^*$, which behaves as the order parameter for the $P2_1/c$-*Pbca* transition.

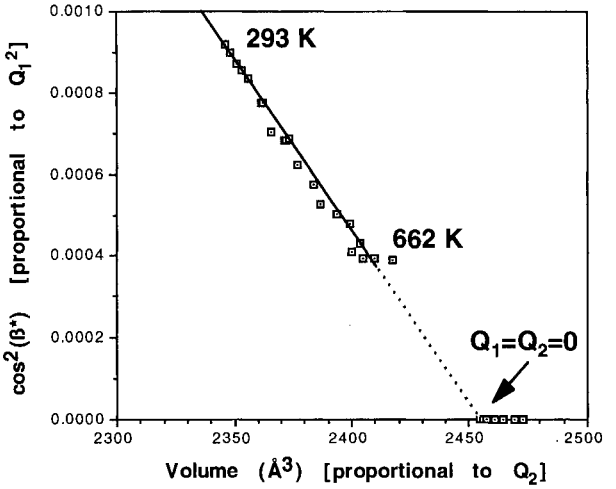

FIGURE 8. Scaling between $\cos \beta^*$ (which may be regarded as the primary ferroelastic order parameter, Q_1) and unit-cell volume (the excess volume behaves as a secondary order parameter, Q_2), demonstrating that $Q_2 \propto Q_1^2$.

ion that appears to control the thermodynamic order of this transition in these materials, and we might expect chemical substitution on the alkali site to modify its character. The volume collapse may be regarded in terms of secondary elastic order parameter, Q_2. Because volume strain is invariant under the action of symmetry operators that are lost upon the phase transition from the high-symmetry paraelastic state to the low-symmetry ferroelastic state (unlike the ferroelastic strain, which changes from $+Q$ to $-Q$ under the operation of these "lost" symmetry elements), volume strain behaves as the square of the primary ferroelastic order parameter, Q_1. This is a general result for any ferroelastic transition and means that the volume strain couples to the primary order parameter, Q_1, through a linear-quadratic term of the form $\lambda Q_1^2 Q_2$, which enters Equation 2 above. A plot of $\cos^2 \beta^*$ against cell volume confirms this linear-quadratic relationship between ferroelastic and volume strain (Fig. 8), showing the linear-quadratic coupling of the two processes.

At higher temperatures, the orthorhombic cell edges tend to converge toward a higher symmetry structure (Fig. 5A). The framework is prohibited from transforming to the cubic phase unless the Mg^{2+} and Si^{4+} cations disorder on the tetrahedral sites (defined by an order parameter Q_{od}). Both Q_{od} and the displacive order parameter for the transition, Q, behave in the same way under the operation of the symmetry elements lost at the transition (they behave as the active representation for the phase transition): They couple bilinearly. Under equilibrium both Q and Q_{od} would fall to zero at T_c on increasing temperature, but this does not appear to happen on the time scale of our high-temperature diffraction experiments because of the kinetic control on cation order-disorder on the tetrahedral sites. If, however, the cell parameters shown in Figure 5 represent those of the equilibrium or near-equilibrium state, and some disorder has occurred, then the extrapolation of the square of the *m*3*mFmmm* scalar spontaneous strain to zero provides an estimate of the temperature of the Mg-Si order-disorder transformation in $K_2MgSi_5O_{12}$. Scalar strain has been defined for the lowest symmetry case by Redfern and Salje (1987). Because it is the magnitude of the spontaneous strain (a second-rank tensor property) that varies critically below a phase transition, the reduction of strain to this scalar quantity provides a convenient measure of an order parameter as a function of temperature. From Figure 9 it thus appears that the transformation to cubic symmetry would occur at 1028 K, but because of the bilinear coupling between Q_{od} and Q and the relatively low temperatures, which make disordering times very long, this transformation has not yet been observed experimentally, not least because $K_2MgSi_5O_{12}$ melts at relatively low temperatures (we have not determined the melting point accurately, but our studies so far suggest that $K_2MgSi_5O_{12}$ melts incongruently at temperatures between 800 and 900 °C). Nonetheless, the dry-synthesized $K_2MgSi_5O_{12}$ leucite analog does show cubic symmetry, even at room temperature, indicating the influence of Q_{od} on the high-temperature and quench behavior of this framework structure. The transition temperature and thermodynamic character of the $P2_1/c$-*Pbca* phase transition are expected to show a strong dependence on Q_{od}. Furthermore, the large strain that Q_{od} induces might be expected to result in the development of tweed microstructures in ordering and disordering experiments on these leucite analogs. These experiments with $K_2MgSi_5O_{12}$ are difficult to conduct because of its low melting point, but investigations into the ordering and disordering of tetrahedral cations in the $Rb_2ZnSi_5O_{12}$ isomorph (which has a higher melting point,

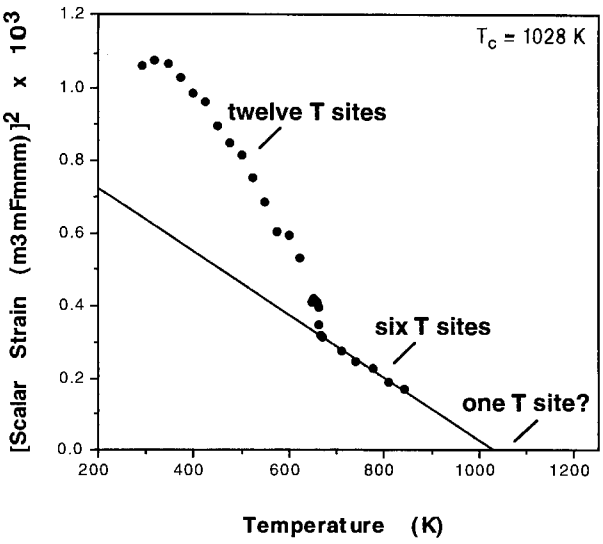

FIGURE 9. Temperature dependence of the square of the orthorhombic distortion from cubic. This strain, the *m3mFmmm* state parameter ($e_s^2 = e_{11}^2 + e_{22}^2 + e_{33}^2$), is proportional to the order parameter for a fictive orthorhombic-cubic phase transition and extrapolates to zero, indicating a transition to cubic at 1028 K (which is above the melting point).

allowing faster Zn-Si exchange kinetics) are currently underway.

It remains to be seen why $K_2MgSi_5O_{12}$ can order its tetrahedral cations but $KAlSi_2O_6$ cannot, despite the higher dilution of the ordering cation (Mg) in the former. The answer is expected to lie in the relative magnitudes of the J_1 and J_2 (nearest- and next-nearest-neighbor) exchange interaction terms. The monoclinic ordered structure of $K_2MgSi_5O_{12}$ reveals that Mg-Mg repulsion acts well beyond nearest- and next-nearest-neighbor tetrahedra as all MgO_4 tetrahedra are separated by two SiO_4 tetrahedra. The MgO_4 tetrahedron is considerably larger than the AlO_4 tetrahedron, leading to an enhanced avoidance rule in $K_2MgSi_5O_{12}$ in comparison with $KAlSi_2O_6$, and this appears to be the most important control on T_c for ordering (and hence kinetic accessibility of ordered and disordered states) in this suite of materials. This illustrates the importance of the relationship between ordering and elastic interactions in framework minerals.

ACKNOWLEDGMENTS

The authors are grateful to Martin Dove and Kenton Hammonds for their patience, help, and advice as we learned how to use the CRUSH program for rigid-unit mode analysis. Part of this work was supported by grants from the Royal Society and the EPSRC. We thank David Palmer for his help in drafting Figure 1 and acknowledge Royal Society (14906) and NERC (GR9/1285) grants awarded to him for the film scanner.

REFERENCES CITED

Aizu, K. (1970) Determination of state parameters and formulation of spontaneous strain for ferroelastics. Journal of the Physical Society of Japan, 28, 706–716.

Bell, A.M.T., Cernick, R.J., Champness, P.E., Fitch, A.N., Henderson, C.M.B., Kohn, S.C., Norledge, B.V., and Redfern, S.A.T. (1993) Crystal structures of leucites from synchrotron X-ray powder diffraction data. Materials Science Forum, 133–136, 697–702.

Bell, A.M.T., and Henderson, C.M.B. (1994) Rietveld refinement of the structures of dry-synthesized $M Fe^{III} Si_2O_6$ leucites (M = K, Rb, Cs) by synchrotron X-ray powder diffraction. Acta Crystallographica, C50, 1531–1536.

Bell, A.M.T., Henderson, C.M.B., Redfern, S.A.T., Cernik, R.J., Champness, P.E., Fitch, A.N., and Kohn, S.C. (1994a) Structures of synthetic $K_2MgSi_5O_{12}$ leucites by integrated X-ray powder diffraction, electron diffraction and ^{29}Si MAS NMR methods. Acta Crystallographica, B50, 31–41.

Bell, A.M.T., Redfern, S.A.T., Henderson, C.M.B., and Kohn, S.C. (1994b) Structural relations and tetrahedral ordering pattern of synthetic orthorhombic $Cs_2CdSi_5O_{12}$ leucite: A combined synchrotron X-ray powder diffraction and multinuclear MAS NMR study. Acta Crystallographica, B50, 560–566.

Brown, I.W.M., Cardile, C.M., MacKenzie, K.J.D., Ryan, M.J., and Meinhold, R.H. (1987) Natural and synthetic leucites studied by solid state 29-Si and 27-Al NMR and 57-Fe Mössbauer spectroscopy. Physics and Chemistry of Minerals, 15, 78–83.

Dove, M.T., Cool, T., Palmer, D.C., Putnis, A., Salje, E.K.H., and Winkler, B. (1993) On the role of Al-Si ordering in the cubic-tetragonal phase transition in leucite. American Mineralogist, 78, 486–492.

Dove, M.T., Thayaparam, S., Heine, V., and Hammonds, K.D. (1996) The phenomenon of low Al-Si ordering temperatures in aluminosilicate framework structures. American Mineralogist, 81, 349–362.

Galli, E., Gottardi, G., and Mazzi, F. (1978) The natural and synthetic phases with the leucite framework. Mineralogica et Petrographica Acta, 22, 185–193.

Hammonds, K.D., Dove, M.T., Giddy, A.P., and Heine, V. (1994) Crush: A Fortran program for the analysis of the rigid-unit mode spectrum of a framework structure. American Mineralogist, 79, 1207–1209.

Heinrich, A.R., and Baerlocher, C. (1991) X-ray Rietveld structure determination of $Cs_2CuSi_5O_{12}$, a pollucite analogue. Acta Crystallographica, C47, 237–241.

Kohn, S.C., Henderson, C.M.B., and Dupree, R. (1994) NMR studies of the leucite analogues $X_2YSi_5O_{12}$, where X = K, Rb, Cs; Y = Mg, Zn, Cd. Physics and Chemistry of Minerals, 21, 176–190.

O'Neill, B., Nguyen, J.H., and Jeanloz, R. (1993) Rapid computer analysis of X-ray diffraction films. American Mineralogist, 78, 1332–1335.

Redfern, S.A.T. (1995) Relationship between order-disorder and elastic phase transitions in framework minerals. Phase Transitions, 55, 139–154.

Redfern, S.A.T., and Salje, E. (1987) Thermodynamics of plagioclase: II. Temperature evolution of the spontaneous strain at the $I\bar{1}$-$P\bar{1}$ phase transition in anorthite. Physics and Chemistry of Minerals, 14, 189–195.

Salje, E.K.H. (1990) Phase transitions in ferroelastic and co-elastic crystals, 366 p. Cambridge University Press, Cambridge.

Torres-Martinez, L.M., and West, A.R. (1989) Pollucite-related and leucite-related phases ($A_2BX_5O_{12}$ and ACX_2O_6; A = K, Rb, Cs; B = Be, Mg, Fe, Co, Ni, Cu, Zn, Cd; C = B, Al, Ga, Fe, Cr; X = Si, Ge). Zeitschrift für anorganische und allgemeine Chemie, 576, 223–230.

MANUSCRIPT RECEIVED MARCH 14, 1995
MANUSCRIPT ACCEPTED NOVEMBER 28, 1995